ARCHIVES OF ELECTRICAL ENGINEERING VOL. 68(2), pp. 357–371 (2019)

DOI 10.24425/aee.2019.128273

Design of a rotor with a starter-generator integrated into an aero car

ZAIXIN WU, RUIGUANG YU

School of Mechanical and Electrical Engineering
Lanzhou University of Technology
Lanzhou 730050, China
e-mail: orinyu@outlook.com

(Received: 30.09.2018, revised: 14.01.2019)

Abstract: The Halbach array structure rotor of the aero motor can satisfy the requirements of high power density and high air-gap flux for aeronautical motors. The size parameters of the rotor are determined by the power rating of the motor based on an analytic method. Producing a Halbach array structure is difficult. Comparison and analysis of the structure of the aero motor show that the overall structure of the rotor adopts a three-axial-section classic Halbach-array hollow structure, and the rotor magnetic steel adopts a discrete structure of 4 blocks per pole and a single 45° magnetisation mode, which reduces the processing difficulty of the rotor magnetic steel. The finite element method was used to analyse the magnetic flux density distribution of the aeronautical motor under various working conditions. The results show that the motor can produce uniform air-gap flux density at various working conditions and present good sinusoidal periodicity. Furthermore, the axial segment did not produce obvious magnetic flux leakage. Finally, considering the eddy current loss of the stator under the rated power-generation condition with high-frequency magnetic field, we conducted coupling analysis of electromagnetic and heat flows to verify that the thermal characteristics of the rotor magnetic steel material could meet the requirements for the aero motor.

Key words: aero motor, air-gap flux density, axial segmentation, electromagnetic and heat flux coupling, Halbach array structure

1. Introduction

At present, aero cars represent an important research subject in many countries. To cope with serious environmental problems, aero cars with electric drive systems have been developed. Research has shown that the energy conversion efficiency of the traditional piston engine and

the gas turbine generator is only 40%, but the energy conversion efficiency of the electric drive system can reach 70% [1]. Therefore, research on the electric drive system is necessary.

The electric drive system is one of the crucial parts of aero cars, and its core component is the motor. The main functions of the aero motor are starting the aero engine and providing electric energy for the aero car as a whole. At the same time, the remaining energy is stored in the battery pack. The motor is subdivided into an axial and radial motor according to its structure type [2]. The problem we have to address in the design process is the light weight of the aero motor because of the harsh environment and its sensitivity to volume and weight, and the high electromagnetic load of the aero motor. An earth permanent magnet has superior magnetic performance and can effectively reduce the volume and weight of the motor. Furthermore, it has a high intrinsic coercive force, can work in a strongly degaussing environment and can form a special rotor structure to achieve high speed; thus, its mechanical properties are suitable for the vibration and shock environment of the aero motor [3–4]. Therefore, a permanent magnet motor with advantages of high efficiency, high power density and high reliability can be widely used in the aviation and military fields.

In 1979, Halbach proposed a permanent magnet structure that can obtain an ideal unilateral magnetic field by arranging the permanent magnets in different directions of magnetisation [5]. The Halbach array structure can achieve the magnetic density distribution of a nearly sinusoidal air gap, and relative to conventional magnetic distribution, it can obtain a larger air-gap flux; it has a perfect magnetic shielding effect that reduces the thickness of the rotor's yoke, thereby effectively decreasing the weight of the motor. The Halbach magnetic structure can produce the strongest magnetic field with a small amount of magnet; thus, it is widely used in the structure of permanent magnet motors [6].

Reference [7] introduced the process of design and electromagnetic performance analysis of the high-speed permanent magnet motor; the study pointed out that the high circumferential speed of the rotor and the high magnetic flux in the stator winding and the iron core determined the difference between the design method of the high-speed permanent magnet motor with that of the conventional motor. Reference [8–10] compared the Halbach structure motor with the conventional structure motor in detail and found that the former had many advantages over the latter; the conclusion was that the parallel magnetisation was better than the radial magnetisation. In reference [11], an analytical method for calculating the magnetic density of Halbach structures under arbitrary magnetisation was proposed; the relationship between the air-gap magnetic density and pole logarithm of the motor, as well as the thickness of the permanent magnet and the magnetisation angle, were analysed. The Halbach structure calculation model of a permanent magnet synchronous motor (PMSM) was established in reference [12]. A design scheme of the rotor core was proposed to further optimise it. To sum up, the traditional high-speed motor body structure and Halbach array structure have been studied extensively. However, because of the difficulty of magnetisation and complexity of the production process, the Halbach structure has not been widely applied to aeronautical motors. Systematic research is lacking on the rotor structure size design and use of materials for the aeronautical motor.

According to the requirements of high power density and high air-gap flux for aeronautical motors, and through comparison between the operating point and environment of the aero and conventional motors, the basic structure of the motor is defined as a radial inner rotor with a

Halbach structure, which can effectively reduce the curb weight of the motor. The power parameters of the motor are determined by the analytical method. The axial segment and magnetising structure of the magnetic pole discretisation structure is proposed, which simplifies the production process of the Halbach structure. Then, the performance of the rotor is verified by computer-aided engineering simulation.

2. Aero motor structure

The working speed of the aeronautical motor is typically greater than 5000 r/min, the circumference speed can reach 150 m/s, and the high frequency of stator winding current and core flux is generally more than 1000 Hz. Thus, the PMSM is often used in aeronautical motors. Depending on the distribution of the rotor, the permanent magnet motor is mainly divided into two basic forms: inner rotor and outer rotor. Owing to the requirement of the high-speed of the aeronautical motor, the permanent magnet motor is mostly used in the form of inner rotor. The permanent magnet synchronous motor with Halbach structure can be classified into an integral type and discrete type according to the structure of the permanent magnet on the rotor, and several new types have been developed [13].

1. Integral type of Halbach structure

The integrated Halbach structure, as shown in Fig. 1(a), uses the continuous sequential magnetisation of the magnetic steel. The air-gap flux density of the integrated Halbach array increases with the increase of the thickness and polar logarithm of the magnet. Compared with the conventional radial structure motor, the air-gap flux density is higher at arbitrary magnet thickness and the polar logarithm. If the stator adopts a certain concentrated non-stack winding structure, then the no-load electromotive force generated by the sloping slot is sinusoidal. Its complex manufacturing process results in a low forming rate; thus, the utilisation rate is low.

2. Discrete type of Halbach structure

The discrete Halbach array is assembled by a magnetic steel block with a specific magnetisation of n parts (n is the number of magnets per pole). As shown in Fig. 1(b), a discrete Halbach structure consists of two pieces of magnetic steel per pole; the air-gap magnetic field is influenced by the number of magnetic steels per pole, and its manufacturing process is relatively simple compared with that of the integrated structure, which is why it is widely applied in the Halbach structure.

3. New type of Halbach structure

A novel double-layer Halbach permanent magnet array structure has been established in China. Each pole of the double-layer array structure includes two axial distribution permanent magnet Halbach arrays, which are arranged alternately in two different shapes. The Halbach array structure is formed in a certain direction of magnetisation, as shown in Fig. 1(c). The structure is easy to optimise and the air-gap flux density with higher sinusoidal degree can be obtained [14].

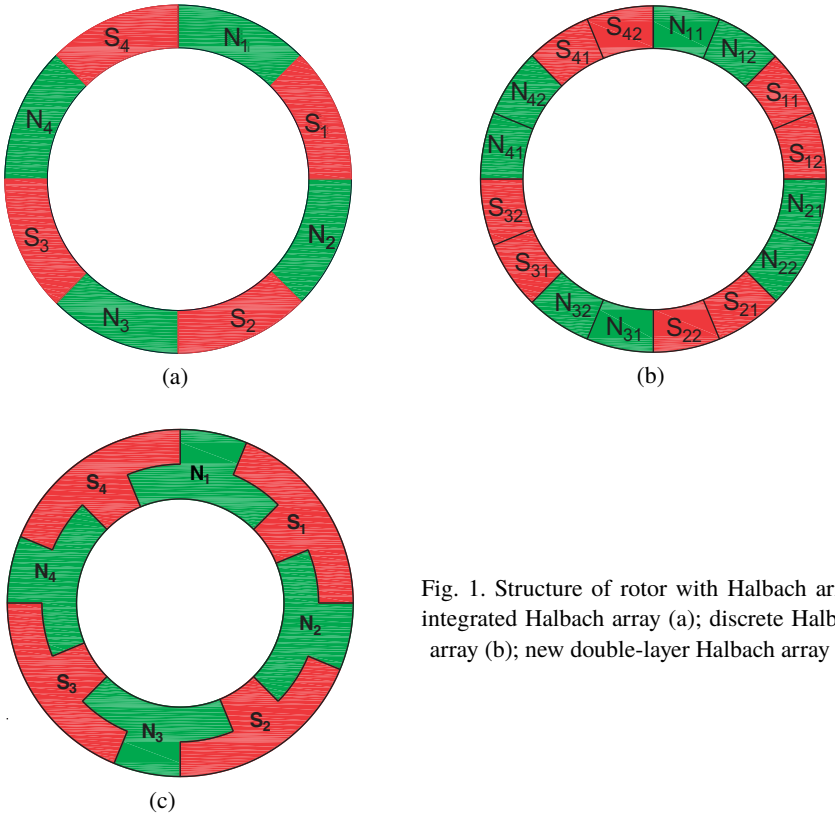

Fig. 1. Structure of rotor with Halbach array: integrated Halbach array (a); discrete Halbach array (b); new double-layer Halbach array (c)

3. Analytical method design of rotor of aero motor

3.1. Outer diameter primary calculation of rotor of aero motor

The armature windings of the PMSM are distributed on the stator, the permanent magnet structure is placed on the rotor, and the working characteristics of the aero motor and ordinary motor are considerably different. The rotor is the core component of the motor structure in the design process, so its diameter is related to the overall performance of the motor. The basic idea of calculating the outer diameter of the rotor is to establish the relationship between the stator diameter and rated power of the motor so that the outer diameter of the rotor can be calculated further. The specific design program is as follows [15, 16]:

1. Determination of winding size

i) Rated current I_N

$$I_N = \frac{P_N}{mU_N \cos\varphi}, \tag{1}$$

where: P_N is the rated power; m is the number of motor phases; U_N is the rated phase voltage; and $\cos\varphi$ is the power factor.

ii) Stator winding size
The section area of the required conductor S'_{Cu} is defined as:

$$S'_{Cu} = \frac{I_N}{J}, \tag{2}$$

where: J is the theoretical current density of the conductor.

iii) Number of pole pairs p

$$p = \frac{60 f_N}{n_N}, \tag{3}$$

where: f_N is the rated frequency and n_N is the rated speed.

iv) Total number of stator grooves Z

$$Z = pmq, \tag{4}$$

where: q is the number of slots occupied by each phase per pair of poles.

v) Number of turns per series W

$$W = \frac{ZW_S}{ma}, \tag{5}$$

where: W_S is the number of turns per component, and a is the number of parallel branches.

vi) Winding factors
The central angle corresponding to the monopole winding θ is expressed as:

$$\theta = \frac{2p\pi}{Z}. \tag{6}$$

vii) Slot pitch τ

$$\tau = \frac{Z}{2p}. \tag{7}$$

viii) Fundamental wave K_{w1}

$$K_{w1} = \sin\left(\frac{y_1}{\tau} \cdot \frac{\pi}{2}\right) \cdot \frac{\sin\frac{q\theta}{2}}{q \sin\frac{\theta}{2}}, \tag{8}$$

where: y_1 is the pitch length.

2. Main dimensions

i) Air-gap flux required per pole $\varphi_{\delta 1}$

$$\varphi_{\delta 1} = \frac{C_i U_N}{4.44 f_N W K_{w1}}, \tag{9}$$

where: C_i is the air-gap potential calculation coefficient, and $C_i = 1.05 \div 1.08$.

ii) Armature inner diameter D

$$D = \sqrt{\frac{2p\varphi_{\delta 1}}{\alpha\pi\lambda B_\delta}}, \tag{10}$$

where: α is the polar arc coefficient, λ is the aspect ratio for the PM motor, $\lambda = 0.4 \div 1.5$, and B_δ is the air-gap magnetic induction intensity.

iii) Armature length L

$$L = \lambda D. \tag{11}$$

iv) Pole pitch τ_1

$$\tau_1 = \frac{\pi D}{2p}. \tag{12}$$

v) Rotor diameter D_2

$$D_2 = D - 2\delta, \tag{13}$$

where: δ is the air gap, which always uses the safety value of mechanical permission, $\delta = 0.5 \div 2.5$ mm.

Thus, the initial calculation of the rotor diameter is complete.

3.2. Characteristics and parameters of rotor of aero motor

The technical requirements for the aero motor to be designed in this study are shown in Table 1.

Table 1. Technical requirements for aero motor

Parameter name	Symbol	Value	Unit
Power rating	P_N	120	kw
Peak power	$P_{\max}$	170	kw
Rated speed	n_N	5500	rpm
Maximum speed	$n_{\max}$	6000	rpm
Rated frequency	f_N	50	Hz
Peak efficiency	η	95	%
Weight	M	< 50	kg
Numbers of phases	m	3	
Power factor	$\cos\varphi$	0.8	
Cooling-down method	Air-cooled and liquid cooling		

The winding of the motor uses three-strand coils in parallel. The polar logarithm is 1. For the three-phase and four-wire connection, to eliminate the tooth harmonics and third harmonics, this study uses a 120° winding. The number of phase slots per pair of poles is taken as 3, that is, the number of slots per pole is fractional slot winding 3/2, which can effectively avoid the strong influence of a harmonic magnetic field on voltage waveforms and reduces the loss of a magnetic surface field. The number of parallel branches is 1, the winding pitch is 4, the calculation coefficient of the air-gap electric potential is 1.07, the pole arc coefficient is 0.8, the aspect ratio is 0.4777 and the air-gap magnetic induction is 0.78 T. The main dimensions of the motor calculated by an analytical method are shown in Table 2.

Table 2. Main parameters of motor

Parameter name	Symbol	Value	Unit
Rated current	I_N	121.97	A
Single-strand winding section	S_{Cu}	1.742×10^{-5}	m^2
Center angle of each phase winding	θ	40	°
Air gap flux per pole	$\varphi_{\delta 1}$	1.2580	Wb
Armature inner diameter	D	216.5	mm
Armature length	L	103.4	mm
Rotor diameter	D_2	214.9	mm
Pole pitch	τ_1	340.1	mm
Armature total slot number	Z	9	
Number of conductors per slot	N_S	8	
Number of turns per element	W_S	4	
Number of series turns per phase	W	12	
Slot pitch	τ	4.5	
Fundamental wave	K_{w1}	0.1106	

3.3. 3D design of rotor of aero motor

According to the previous description of the rotor structure of a high-speed motor, the structure of a new hollow rotor with the embedded shaft of the three axial segmentation classic Halbach-array hollow structure is proposed, which can meet the basic requirements of high power density and high air-gap flux. For the Halbach ring array structure in this paper, the permanent magnet is divided into three sections in the axial direction. The 3D Halbach rotor structure motor is shown in Fig. 2. Protecting the permanent magnet is necessary because of its poor tensile strength. In this study, carbon fibre is used to bind the permanent magnet, thereby also preventing high-frequency eddy current loss.

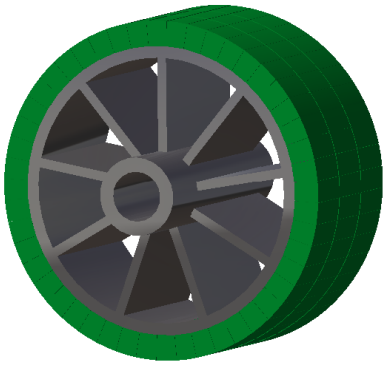

Fig. 2. Structure of rotor with axial three section Halbach array

The magnetisation mode is 45°, as shown in Fig. 3. The magnetisation mode of the Halbach structure is 1/4, and the complete finite element analysis model is presented in Fig. 4.

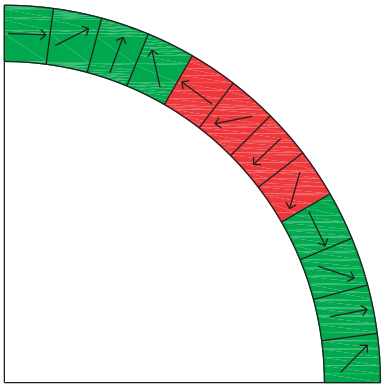

Fig. 3. 45° magnetisation of Halbach array

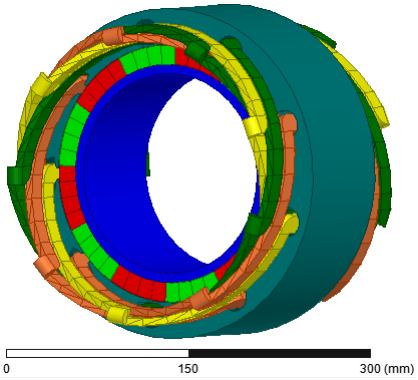

Fig. 4. Finite element analysis model of Halbach axial three-segment array motor

4. Finite element verification of electromagnetic and material properties

The finite element analysis method of a 2D electromagnetic field is mainly based on Maxwell's equations, and the magnetic vector position $\boldsymbol{A}$ in the potential function is used in the analysis. In the 2D magnetic field solver, the field equation that satisfies the vector magnetic potential A is as follows:

$$\nabla \times v \times A = J_s - \sigma \frac{\partial A}{\partial t} - \sigma \nabla v - \nabla \times H_c + \sigma v \times \nabla \times \boldsymbol{A}, \tag{14}$$

where: H_c is the coercivity of the permanent magnet, v is the moving speed of the object, σ is the dielectric conductivity, and J_s is the source current density.

The commonly used boundary conditions in the solution process mainly include the Dirichlet boundary and Neumann boundary conditions, as shown in Formulas (15) and (16), respectively.

$$\varphi|_\Gamma = g(\Gamma), \tag{15}$$

where: Γ is the Dirichlet boundary condition, and $g(\Gamma)$ is the position function that can be constant and zero. This boundary condition defines the distribution of potential at the boundary.

$$\left.\frac{\partial\varphi}{\partial n}\right|_{\Gamma} + f(\Gamma)\varphi|_{\Gamma} = h(\Gamma), \tag{16}$$

where: Γ is the Neumann boundary condition; $f(\Gamma)$ and $h(\Gamma)$ are the general functions, which can be constant and zero. This boundary condition specifies the distribution of the normal derivative of potentials at the boundary.

The edge method is used in the 3D magnetic field analysis to calculate the degree of freedom by the field quantity to be solved on the edge of the subdivision unit. The 3D non-conductive and conductive regions are calculated by Formulas (17) and (18), respectively.

$$H = H_p + \nabla\varphi, \tag{17}$$

$$H = H_p + \nabla\varphi + \boldsymbol{T}, \tag{18}$$

where: φ is the scalar potential on the node, H_p is the intensity of the vector magnetic field on the edge, and $\boldsymbol{T}$ is the vector potential of the edge. The tangential component of the vector potential $\boldsymbol{T}$ at the interface between the conducting and non-conductive regions is forced to be set to 0. The degree of freedom to be solved on this tetrahedron is 10, of which 4 are scalar potentials on 4 vertices of the tetrahedron, and 6 are vector magnetic field intensities on 6 edges of the tetrahedron. Quadratic interpolation approximation is used to solve the field quantity in a single subdivision unit. The 2D boundary conditions are also applicable to 3D magnetic field analysis. In addition, the radiation boundary condition is used in 3D analysis. This boundary condition is used to simulate the case where the magnetic field dispersion should be considered, that is, the magnetic field is zero at infinity.

For the region discretisation in 3D finite element analysis, firstly, the volume V is divided into a certain number of tetrahedron elements, and the S plane is divided into many triangular elements. Then, one set of integers is numbered by volume units and the other by each node of tetrahedron vertices. The $4\times N$ integer array $\boldsymbol{x}(i, j)$ is used to correlate the units with node coding, where $i = 1, 2, 3, 4$; $j = 1, 2, 3, 4, \ldots, N$; and N is the total number of volume units, which store the global node encoding of the i node in the j unit. The integral array $\boldsymbol{xy}(k)$ is further introduced to store the global node codes of nodes on the surface S_1, where $k = 1, 2, 3, 4, \ldots, N_1$; and N_1 is the total number of such nodes. Thus, the Dirichlet boundary is added.

4.1. Distribution of air-gap magnetic flux density under operating conditions of motor

The main flying altitude of the aero car designed in this study is approximately 3 km, and the motor is used in a harsh working environment. According to the requirement of high power density and high-temperature resistance of the aero motor, samarium cobalt permanent magnet (brand number SmCo28) is used. Table 3 shows its material properties, which meet the basic requirements of magnetic energy density, efficiency and temperature. The stator core adopts a soft magnetic alloy (brand number 1J22) with high-saturation magnetic induction strength, which can effectively reduce the high-frequency iron consumption and increase the torque density. The hysteresis loss coefficient kh is 244.40, the eddy current loss coefficient kc is 0.18 and

the additional loss coefficient ke is 0. In addition, the brand number used for the rotor shaft is Ti-6Al-4V, which has a yield strength of 750 MPa, and is characterised by corrosion resistance and high-temperature resistance. The brand number used to support the structure of magnets is Al-MS89, which has a yield strength of 250 MPa; thus, all the materials can meet the requirements of the rotor support structure under high temperature.

Table 3. SmCo28 material properties

Parameter name	Value	Unit
Coercive force	342	KA/m
Working temperature	350	°C
Curie point	820	°C
Remanent magnetic density	0.53	T
Maximum magnetic energy pro	52	KJ/m^3
Intrinsic coercivity	796	KA/m

In the solution of a 3D magnetic field, the relative coordinate system is established for each magnet, and the material definition of each magnet is conducted according to the magnetisation method in Fig. 3. The initial conditions are applied with a current excitation source and infinite far-field boundary condition. For each piece of the magnet, the mesh method based on skin effect is used to effectively simulate the changing trend of the magnetic field in the penetration depth, and the air-gap region is treated by divisional modularisation, that is, discretisation. Each module is processed by radial stratification encryption to improve the accuracy of the solution. The parallel boundary condition vector potential of magnetic flux is applied in the 2D magnetic field solution, and the rotation motion option is set in the rotor. The solution terminal time is 0.04 s and the solution step is 0.0002 s.

The frequently used operating condition of the aero motor is a power generation condition. Therefore, the distribution of magnetic flux density in steady-state generation of the motor is obtained, as shown in Fig. 5. The magnetic field waveforms in an axial, radial and air gap are shown in Figs. 6(a), (b), (c), respectively. Fig. 5(a) shows that the rotor radial magnetic steel can produce more than 1 T flux density, and the maximum magnetic flux density is 2.71 T. Figs. 5(b) and 6(a) show that the axial section does not produce magnetic flux leakage in the axial gap, it has good continuity of axial flux density, and the difficulty of the magnetic steel production is greatly reduced. The entire motor can produce uniform flux density, and local magnetic leakage is found under the yoke of the magnetic steel, which are mainly due to the discontinuity of the local magnetisation direction, the magnetic leakage between the magnetic blocks and the rotor yoke, and the limited axial length of the magnet. Fig. 6(b) shows that the radial magnetic field waveform is continuous and smooth. Fig. 6(c) shows the magnetic field waveform in the air gap, which is very close to sinusoidal characteristics. The preceding results show that the designed Halbach structure has good reliability.

The main operating conditions of the aero motor are start-up, no-load idling and rated power generation. The distribution of air-gap magnetic flux density is presented in Fig. 7. Fig. 7(a) shows that the rotor's speed at the start-up condition is low but the rotor needs to overcome 1.7 times rated

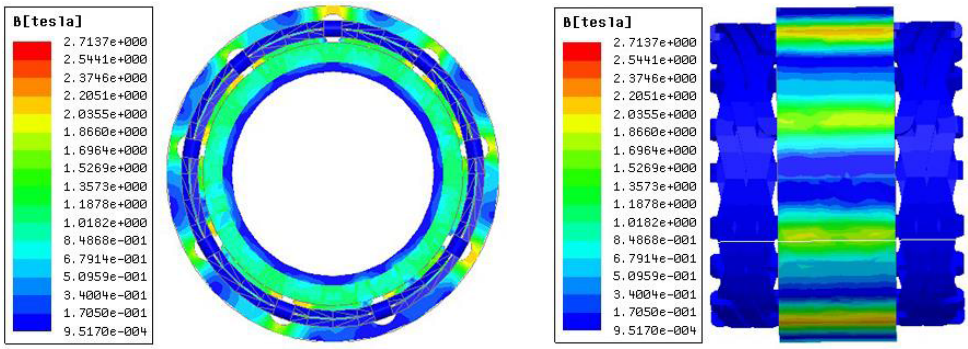

(a) (b)

Fig. 5. Magnetic flux density distribution under steady-state power generation of motor: 3D Radial (a); 3D Axial (b)

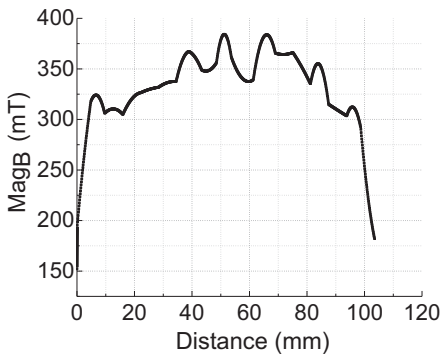

(a)

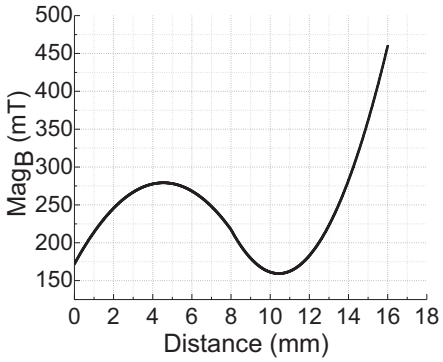

(b)

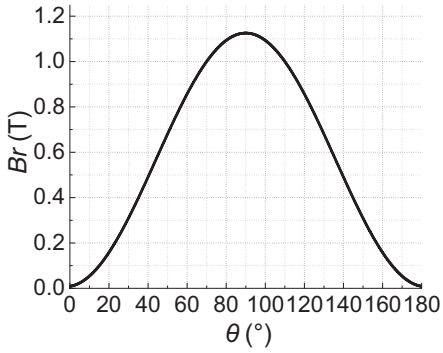

(c)

Fig. 6. Magnetic field waveforms: axial (a); radial (b); air gap (c)

torque to start, the outer edge of the magnetic steel produces the strongest magnetic flux density, the highest magnetic flux density is 2.98 T and the overall flux density is evenly distributed. Fig. 7(b) shows that magnetic flux leakage occurs in the produced flux density above 0.7 T.

Fig. 7(c) shows that the overall magnetic flux density of the steel underrated power generation condition can produce 1 T flux density, which is almost the same as the magnetic flux density generated under 3D conditions in the previous section, and the overall flux density is uniformly distributed. We can observe in Fig. 7 that the motor can produce uniform air-gap magnetic flux density under all working conditions, exhibits good periodicity and meets the actual working condition requirements for the aero motor.

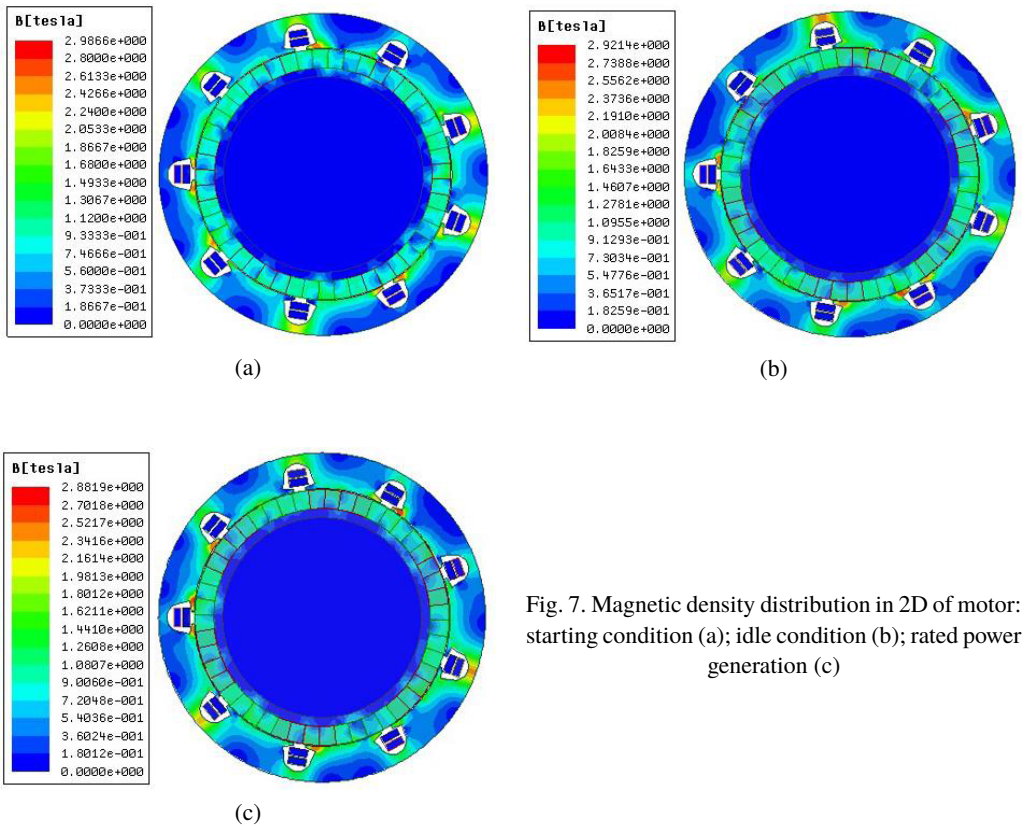

Fig. 7. Magnetic density distribution in 2D of motor: starting condition (a); idle condition (b); rated power generation (c)

4.2. Temperature distribution of magnetic steel underrated power generation condition

This motor has high power density, and the rotor is cooled by forced air cooling. To reduce the thermal radiation from the stator to the rotor, the entire stator is encapsulated. Considering the eddy current loss of the stator in the high-frequency magnetic field underrated generation condition, we conduct electromagnetic heat-flux coupling analysis of the motor.

On the premise of guaranteeing the original heat consumption power and cooling air volume, the model is simplified to enhance calculation convergence and stability and therefore improve calculation accuracy [17]. In the coupling analysis, the eddy current loss value 107.66 w is shared with the fluid analysis model by volumetric energy source in EM mapping. The calculated

temperature of the permanent magnet is shown in Fig. 8. The ambient and inlet air temperature are both 100°C, and the maximum working temperature of magnetic steel is 350°C. The maximum temperature of the magnetic steel is 182.7°C on the axial surface. The wind volume increases layer by layer so that the axial surface temperature is higher than the axial back-end temperature. The results show that the material characteristics of the magnetic steel and the forced air cooling of the rotor can meet the cooling requirements.

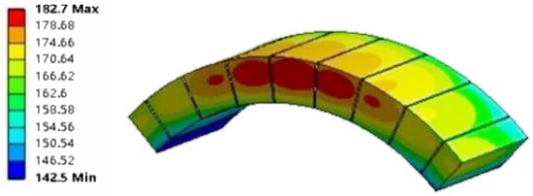

Fig. 8. Temperature distribution of permanent magnet of Halbach array

The rotor component mass is calculated as shown in Table 4. Compared with the overall mass requirement of the motor in Table 1, the rotor mass is only 21.58% of the total required mass. The results show that the embedded hollow shaft structure of the classical Halbach structure can effectively reduce the mass of the motor. Thus, the unit power density of the motor is raised to meet the design requirements.

Table 4. Rotor's material properties

Structure name	Density	Unit	Mass	Unit
Permanent magnet	8310	kg/m^3	7.30	kg
Spiale	4430	kg/m^3	2.13	kg
Permanent magnet supporting structure	2930	kg/m^3	1.36	kg
Rotor total mass			10.79	kg

5. Conclusions

By analysing the working characteristics of an aero motor, and on the premise of satisfying the high power density and high air-gap flux of the aeronautical motor, the rotor with the embedded shaft structure of the Halbach classic-array hollow structure is designed for the starter-generator integrated into the aero car. The following conclusions are obtained:

1) According to the working characteristics of the aero motor, the three-axial-section classic Halbach-array structure of a rotor can cut down the axial processing difficulty of magnetic steel; thus, the problem of axial magnetisation discontinuity in Halbach is solved. In addition, the method of 45° radial magnetisation in 4 blocks per pole of the Halbach discrete structure reduces the magnetising difficulty. The method can produce strong and periodic air-gap flux density, and does not generate obvious magnetic flux leakage in the axial segment, thereby meeting the aero motor requirements under various working conditions.

2) Coupling analysis of electromagnetic and heat flux was conducted between the severe high-temperature environment and the influence of eddy current loss value of the stator in a high-frequency magnetic field on the overall heat flux of the aeronautical motor. We verified that the forced air cooling of the rotor meets the heat dissipation requirement of magnetic steel. Thus, the selection of magnetic steel materials meets the design requirements.

3) The Halbach rotor without a yoke and hollow structure embedded shaft effectively reduces the rotor mass and meets the high-power density requirements for the aero motor. Finally, the rotor structure selection, dimension parameter calculation and material used in this study provide a reference for the rotor design of an aeronautical motor in the future.

4) In the next stage of our work, other challenges to system weight loss are acoustic noise and vibration. The vibration modes of the system are calculated and simulated to determine the frequency points. Owing to the long manufacturing period of the motor, the manufacturer is currently producing customised motors, and the accuracy of the calculation cannot be verified.

References

[1] Zhang Z., Yu L., Li J. *et al*., *Key technologies of advanced aircraft electrical machine system for aviation electrification*, Journal of Nanjing University of Aeronautics & Astronautics, vol. 49, no. 5, pp. 622–634 (2017).

[2] Huang Y., Zhang T., Dong J. *et al*., *An overview on developments and research of axial flux permanent magnet machines*, Proceedings of the CSEE, vol. 35, no. 1, pp. 192–205 (2015).

[3] Li Z., Chen F., *Rare-earth permanent magnet motor*, Aeronautical Science and Technology, pp. 19–22 (1996).

[4] Qiu H., Yu W., Li Yi. *et al*., *Research on the influence of driving harmonic on electromagnetic field and temperature field of permanent magnet synchronous motor*, Archives of Electrical Engineering, vol. 66, no. 2, pp. 295–312 (2017).

[5] Zhang Y., Qiao D., Gao J., *Current research on and applications of halbach permanent magnet array*, Analytical Instrumentations/Fen xi Yi qi, no. 2, pp. 5–10 (2010).

[6] Shi T., Qiao Z., Xia C. *et al*., *Modeling analyzing, and parameter design of the magnetic field of a segmented Halbach cylinder* [J], IEEE Transactions on Magnetics, vol. 48, pp. 1890–1898 (2012).

[7] Wang J., Wang F., Kong X., *Design and analysis of electromagnetic properties for high speed PM generator*, Proceedings of the CSEE, vol. 28, no. 20, pp. 105–110 (2008).

[8] Xu Y., Yao F., Fang J., *Halbach array permanent magnet machine and performance comparison with the normal array one (I) – Halbach array structure and comparison of different magnet array machines*, Transactions of China Electrical Society, vol. 19, no. 2, pp. 79–83 (2004).

[9] Xu Y., Yao F., Fang J., *Halbach array permanent magnet machine and its performance comparison with the normal array one (II) – comparison of different magnet array ironless machine and prototype experiment*, Transactions of China Electrotechnical Society, vol. 19, no. 6, pp. 58–62 (2004).

[10] Zhu H., Chen L., Li Y. *et al*., *Finite element analysis of bearingless permanent magnet motors with Halbach array*, Electric Machines and Control, vol. 17, no. 4, pp. 45–49 (2013).

[11] Liang J., Zhang X., Qiao M. *et al*., *Analytic model of discrete random magnetizing halbach PM motor*, Acta Phys. Sin., vol. 62, no. 15, pp. 39–47 (2013).

[12] Wang A., Zhu J., Shang Y., *Optimization of iron core design for permanent-magnet synchronous machines with three-segment halbach magnet array*, Electric Machines and Control, vol. 21, no. 4, pp. 37–43 (2017).

[13] Zhu D., Yan Y., *Features of airgap flux density in segmented halbach permanent magnet synchronous motor and itd no-load EMF waveform optimization*, Transactions of China Electrotechnical Society, vol. 23, no. 11, pp. 22–27 (2008).

[14] Kou B., Cao H., Li W. *et al*., *Analytical analysis of a novel double layer halbach permanent magnet array*, Transactions of China Electrotechnical Society, vol. 30, no. 10, pp. 68–76 (2015).

[15] Li Z., Liu W. *et al*., *Rare earth permanent magnet motor*, National Defense Industry Press (2015).

[16] Dai W., Zhang J. *et al*., *Motor design* [M], Tsinghua University Press (2010).

[17] Fasquelle A., Laloy D., *Water cold plates cooling in a permanent pagnet synchronous motor*, IEEE Transactions on Industry Applications, no. 53, pp. 4406–4413 (2017).